Communication

Functional Integrity of Radical SAM Enzyme Dph1•Dph2 Requires Non-canonical Cofactor Motifs with Tandem Cysteines

Koray Ütkür , Klaus Mayer , Shihui Liu , Ulrich Brinkmann , Raffael Schaffrath [*]

Communication

Functional Integrity of Radical SAM Enzyme Dph1•Dph2 Requires Non-Canonical Cofactor Motifs with Tandem Cysteines

Koray Ütkür [1], Klaus Mayer [2], Shihui Liu [3], Ulrich Brinkmann [2] and Raffael Schaffrath [1,*]

[1] Institut für Biologie, Fachgebiet Mikrobiologie, Universität Kassel, 34132 Kassel, Germany; k.uetkuer@uni-kassel.de (K.Ü.); schaffrath@uni-kassel.de (R.S.)

[2] Roche Pharma Research and Early Development (pRED), Large Molecule Research, Roche Innovation Center Munich, Penzberg, Germany; klaus.mayer.km1@roche.com (K.M.); ulrich.brinkmann@roche.com (U.B.)

[3] Division of Infectious Diseases, Department of Medicine, University of Pittsburgh School of Medicine, Pittsburgh, PA, USA; shl176@pitt.edu (S.L.)

[*] Correspondence: schaffrath@uni-kassel.de; Tel.: +49-561-804-4175

Abstract: The Dph1•Dph2 heterodimer from yeast is a radical SAM (RS) enzyme that generates the 3-amino-3-carboxy-propyl (ACP) precursor for diphthamide, a clinically relevant modification on eukaryotic elongation factor 2 (eEF2). ACP formation requires SAM cleavage and atypical Cys-bound Fe-S clusters in each Dph1 and Dph2 subunit. Intriguingly, the first Cys residue in each motif locates next to another, ill-defined cysteine that we show in-here is conserved across eukaryotes. As judged from structural modeling, the orientation of these tandem cysteine motifs (TCM) suggests a candidate Fe-S cluster ligand role. Hence, we generated by site-directed *DPH1* and *DPH2* mutagenesis, Dph1•Dph2 variants with cysteines from each TCM replaced individually or in combination by serines. Assays diagnostic for diphthamide formation *in vivo* reveal that while single substitutions in the TCM of Dph2 cause mild defects, double mutations almost entirely inactivate the RS enzyme. Based on enhanced Dph1 and Dph2 subunit instability in response to cycloheximide chases, the variants with Cys substitutions in their cofactor motifs are particularly prone to protein degradation. In sum, we identify a fourth functionally cooperative Cys residue within the Fe-S motif of Dph2 and show that the Cys-based cofactor binding motifs in Dph1 and Dph2 are critical for the structural integrity of the dimeric RS enzyme *in vivo*.

Keywords: Dph1•Dph2; radical SAM enzyme; iron sulfur cluster; cysteine ligands; eEF2; diphthamide modification; ADP-ribosylation; *Saccharomyces cerevisiae*

1. Introduction

Radical SAM (RS) enzymes contain iron-sulfur (Fe-S) cluster cofactors associated with reductive cleavage of S-adenosyl-methionine (SAM) and formation of classical 5'-deoxyadenosine (dAdo) radicals [1,2]. These are used for H-atom abstraction from substrates in a plethora of cellular syntheses including but not limited to modifications of biomacromolecules [1-3]. Classical members of the RS family share a radical SAM motif (CX_3CX_2C) with each cysteine coordinating one iron of the cofactor, usually a cubic [4Fe-4S] cluster. The fourth, unique iron binds SAM to set the catalytic framework of a site-differentiated Fe-S cluster for reductive SAM cleavage [3,4]. The Cys-bound Fe-S clusters not only are crucial for SAM catalysis, but also for RS enzyme structure and stability. Hence, mutation of crucial cysteines in the SAM motif can induce Fe-S cluster loss as well as enzyme inactivation or degradation [5,6].

Apart from classical RS enzymes, there are non-canonical ones, i.e., eukaryotic Dph1•Dph2 and archaeal Dph2•Dph2 orthologs, that significantly differ with regards to subunit composition, Fe-S cluster coordination, SAM cleavage and radical formation [7-10]. Dph1•Dph2 processes SAM into a non-canonical 3-amino-3-carboxy-propyl (ACP) radical used for modification of eukaryotic

translation elongation factor 2 (eEF2) with diphthamide [11-13]. Diphthamide is formed by a dedicated synthesis network (i.e., Dph1-Dph8) on a conserved histidine of eEF2 in eukaryotes (His-699 in budding yeast *Saccharomyces cerevisiae* and His-715 in *Homo sapiens*) and EF2 in some archaea [14-17]. Importantly, human patients deficient in diphthamide-modified eEF2 display symptoms of a neurodevelopmental disorder known as diphthamide deficiency syndrome (DDS) [18-22] and diphtheria toxin (DT) from *Corynebacterium diphtheriae* attacks the diphthamide décor on eEF2 by ADP-ribosylation to block mRNA translation in infected host cells [23]. Yeast diphthamide mutants (i.e., *dph1Δ–dph8Δ*) are resistant to eEF2 and growth inhibition by DT, which is why the toxin is a valuable molecular tool to tell diphthamide proficiency from deficiency *in vivo* [17,24].

The yeast Dph1•Dph2 heterodimer contains one Fe-S cluster per subunit , yet both Dph1 and Dph2 lack the consensus (CX_3CX_2C) typical of classical radical SAM domains [9,10]. Instead Fe-S cluster coordination relies on atypical Cys-based motifs in Dph1 ($CX_{105}CX_{129}C$) and Dph2 ($CX_{21}CX_{234}C$), which upon mutation cause Fe-S cluster loss and diphthamide defects [9,10] and importantly, are verified triggers of DDS [21]. Intriguingly, there are other ill-defined cysteines: Dph1Cys-134 and Dph2Cys-106. Both form tandem cysteine motifs (TCM) with Cys residues previously implicated in Fe-S cluster binding: Dph1Cys-133 and Dph2Cys-107 [9,10]. As judged from sequence alignments with other eukaryotic Dph1 and Dph2 subunits and structural Dph1•Dph2 modeling, we show in-here the TCMs are conserved from yeast to man and possibly expand the atypical Cys-based cofactor binding motifs. Therefore, we generated *DPH1* and *DPH2* gene substitutions for functional analysis of site-specific Cys-to-Ser variants in either Dph1 or Dph2. Assays diagnostic for diphthamide synthesis reveal that while replacement of either Cys-106 or Cys-107 alone in Dph2 had mild effects, their combined substitution almost entirely abolished Dph1•Dph2 activity. Furthermore, we show that irrespective of position, replacing essential cysteine ligands from SAM and/or Fe-S binding motifs in Dph1 or Dph2 results in accelerated decay of both subunits unanimously. Collectively, our data establish the relevance of TCMs and Cys-based motifs in Dph1 and Dph2 as factors that determine the function and structural integrity of the Dph1•Dph2 dimer.

2. Materials and Methods

2.1. Strains, Media & Cell Growth Conditions

The *S. cerevisiae* strains used or generated throughout this study are listed in Table S1. BY4741-derived yeast strains carrying site-specific substitution or deletion mutations at *DPH1* or *DPH2* chromosomal loci were generated using PCR-mediated protocols, oligonucleotides, gene-specific primers (Table S2) and plasmid templates as previously described [10,24,25] HA or c-Myc epitope tagging at wild-type and mutant *DPH1* or *DPH2* loci for Dph1 or Dph2 gene product detection involved previously described PCR-methods [26]. DNA transformations utilized standard lithium-acetate protocols [27], and strains were grown in complete yeast peptone dextrose (YPD) or minimal synthetic defined (SD) media [28] at 30 °C. For antifungal response assays, ten-fold serial cell dilutions of *S. cerevisiae* tester strains (starting OD_{600}: 1.5) were spotted on YPD plates lacking or containing 5-15 µg/mL sordarin (Sigma-Aldrich) and incubated for 2-4 days at 30°C. As previously described [24], DT response assays used transformation with a plasmid (pSU9) for galactose induction of the cytotoxic ADP-ribosylase domain of DT.

2.2. Dph1•Dph2 Sequence Alignments and Modeling Based on Archaeal Dph2 Structures

The sequence of *Pyrococcus horikoshii* (*Ph*) Dph2 (UniProt-ID O58832) was aligned to Dph1 and Dph2 from *S. cerevisiae* (*Sc*) (UniProt-IDs P40487 and P32461), *Arabidopsis thaliana* (*At*) (UniProt-IDs Q8RWW3 and A0A1I9LRW3), *Drosophila melanogaster* (*Dm*) (UniProt-IDs Q9VTM2 and Q9VFE9), *Mus musculus* (*Mm*) (UniProt-IDs Q5NCQ5 and Q9CR25) or *Homo sapiens* (*Hs*) (UniProt-IDs Q9BZG8 and Q9BQC3) using ClustalOmega (https://www.ebi.ac.uk/Tools/msa/clustalo/ accessed on 5th February 2024) and illustrated via Jalview (https://www.jalview.org/development/archive/Version-2_11_2_7/ accessed on 5th February 2024). AlphaFold/ColabFold [29,30] based models of Dph1•Dph2

were guided by the solved structure of *Ph*Dph2 (PDB:3LZD) [7,12] as described [10,21] (https://colab.research.google.com/github/sokrypton/ColabFold/blob/main/AlphaFold2.ipynb accessed on 5th February 2024). Structure visualization used PyMOL (https://pymol.informer.com/1.3/ accessed on 5th February 2024), and the cysteine residues of the atypical radical SAM and/or Fe-S binding motifs were curated manually.

2.3. Assaying Diphthamide-Modification of eEF2 and ADP-Ribosylation (ADPR) by ETA

Diagnosis of eEF2 diphthamide modification states *in vivo* involved Western blots of total yeast cell extracts with antibodies that recognize global eEF2 pools irrespective of diphthamide modification (anti-eEF2[pan]) or unmodified forms of eEF2 (anti-eEF2[no diphthamide]) [31]. Both antibodies were originally raised to detect human eEF2. As the diphthamide acceptor contexts in eEF2 from human and yeast cells are identical, anti-EF2(no diphthamide) can also differentiate the modification states of eEF2 in *S. cerevisiae* [32] and in plants as recently shown [33]. Unmodified eEF2 signals relative to *dph1Δ* or *dph2Δ* were quantified using densitometry with ImageJ version 1.50i. Yeast cell extracts were generated as described [34] and protein concentrations determined by the Bradford assay [35]. Lämmli samples were run by SDS-PAGE (12% [*w/v*] polyacrylamide) and blotted onto PVDF membranes (Millipore, Burlington, MA, USA). These were probed overnight at 4 °C with the anti-eEF2(pan) and anti-eEF2(no diphthamide) antibodies and developed using anti-rabbit secondary antibody horseradish-peroxidase conjugates (Dianova, Hamburg, Germany; working concentration: 1/5,000) and Lumi-Light Western blotting substrate (Roche, Basel, Switzerland) as described [10,21,32]. Protein loading was controlled in parallel with anti-Cdc19 antibodies (kindly donated by Prof. Jeremy Thorner, University of California, Berkeley, CA, USA) recognizing yeast pyruvate kinase. Similarly, anti-HA Western blots (Invitrogen, Waltham, MA, USA) were performed to detect HA-tagged Dph1 proteins, and anti-c-Myc Western blots (9E10 antibody kindly donated by Prof. Markus Maniak, University of Kassel, Germany) confirmed expression of c-Myc-tagged Dph2 proteins. Cycloheximide chases followed a previously described protocol [36]. In brief, yeast was grown overnight to inoculate (OD_{600}: 0.5) main cultures for 3h until exponential phase prior to cycloheximide [100 μg/ml] addition. Fractions of cultures were taken before (0 h) and up to nine h after cycloheximide treatment followed by Western blot analysis as above. Diphthamide-dependent ADPR acceptor activity of eEF2 in presence of *Pseudomonas aeruginosa* exotoxin A (ETA), an ADP-ribosylase similar to DT [23], was tested *in vitro* using yeast extracts and biotinylated NAD^+ as ADP-ribosyl donor for ETA and a streptavidin-peroxidase conjugate (Roche, Basel, Switzerland) to detect ADPR on eEF2 [24,37].

3. Results and Discussion

3.1. Tandem Cysteine Motifs (TCM) in Dph1 and Dph2 are Conserved from Yeast to Humans

Atypical cofactor binding motifs from Dph1•Dph2 have been identified elegantly in *S. cerevisiae* based on sequence conservation between its archaeal Dph2•Dph2 ortholog from *P. horikoshii* (*Ph*), whose crystal structure has been solved [7,9,12]. Intriguingly, Dph1 and Dph2 sequences from yeast (but not *Ph*Dph2) revealed that the first Fe-S cluster binding cysteine is next to another one of unknown relevance. Thus, in Dph1 uncharacterized Cys-134 is in tandem with Fe-S cluster ligand Cys-133, and a similar scenario applies to Dph2 with ligand Cys-106 adjacent to Cys-107 [9,10]. Since their significance is unclear, we examined whether TCMs are unique to yeast or found in other eukaryotes and aligned Dph1 and Dph2 sequences between *S. cerevisiae* (*Sc*), *A. thaliana* (*At*), *D. melanogaster* (*Dm*), *M. musculus* (*Mm*), and *H. sapiens* (*Hs*) (Figure S1). Compared to *Ph*Dph2, which displays a Cys-Asp motif, all eukaryal Dph1 and Dph2 sequences tested, carry a Cys residue in position 1 of the Fe-S cluster motif that indeed forms a conserved TCM (Figure 1A). We modeled the yeast Dph1•Dph2 dimer with AlphaFold using the solved structure of *Ph*Dph2 to further characterize the cryptic Cys residues in each TCM (Figure 1B). The model identifies both verified and potential Fe-S cluster ligands [9] in Dph1 (Cys-133; Cys-239; Cys-368) and Dph2 (Cys-107; Cys-128; Cys-362) (Figure 1B, middle and right panels), in line with those from *Ph*Dph2 (Cys-59; Cys-163; Cys-287)

(Figure 1B, left panel). Strikingly, the cryptic cysteines in each TCM (i.e., Dph1Cys-134 and Dph2Cys-106) also are oriented towards the Fe-S cofactors, suggesting they may qualify as candidate ligands (Figure 1B, middle and right panels). In contrast, Asp-60 next to Fe-S cluster ligand Cys-59 in *Ph*Dph2, faces away from the cofactor (Figure 1B, left panel). In sum, we surmised that four rather than three cysteines may the atypical cofactor motifs in Dph1 ($CCX_{105}CX_{129}C$) and Dph2 ($CCX_{21}CX_{234}C$) (Figure 1B) and function as candidate Fe-S ligands.

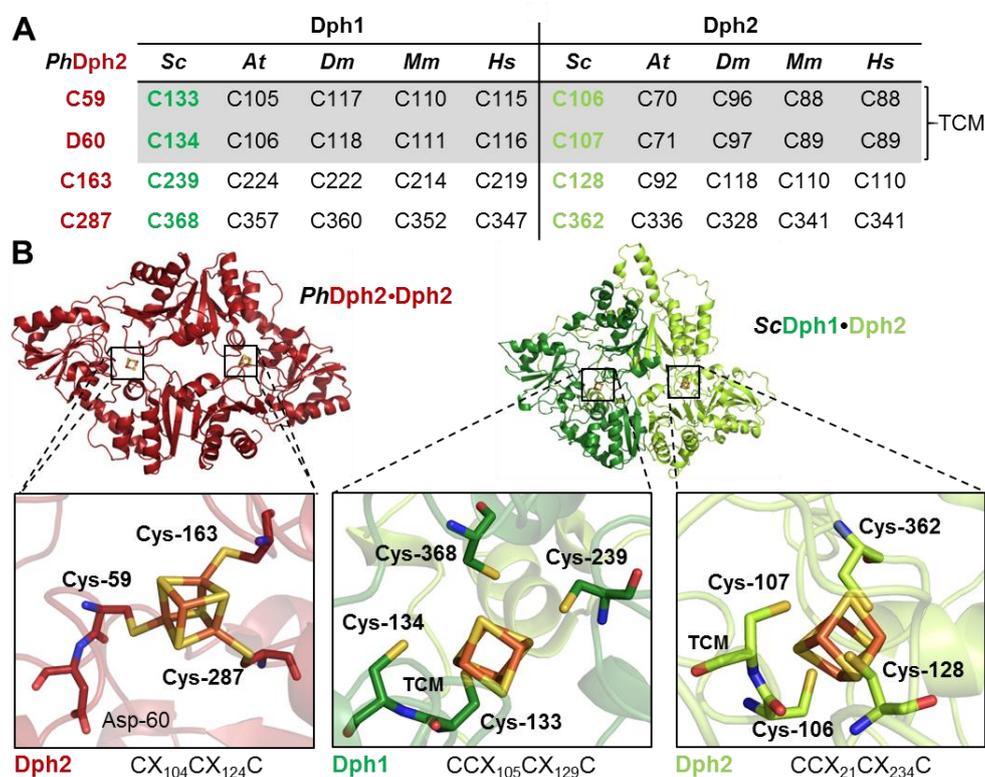| A		Dph1					Dph2				
*Ph*Dph2	*Sc*	*At*	*Dm*	*Mm*	*Hs*	*Sc*	*At*	*Dm*	*Mm*	*Hs*	
C59	C133	C105	C117	C110	C115	C106	C70	C96	C88	C88	⎤
D60	C134	C106	C118	C111	C116	C107	C71	C97	C89	C89	⎦ TCM
C163	C239	C224	C222	C214	C219	C128	C92	C118	C110	C110	
C287	C368	C357	C360	C352	C347	C362	C336	C328	C341	C341	

Figure 1. TCM conservation in atypical radical SAM and Fe-S motifs from Dph1•Dph2 dimers. (**A**) Dph1 and Dph2 alignment from indicated eukaryotic species to archaeal Dph2 (for full details, see Figure S1). (**B**) Structural comparisons. Left: Structure of the *Ph*Dph2•Dph2 homodimer (firebrick red; PDB:3LZD) with the Cys-based (Cys-59; Cys-163; Cys-287) Fe-S binding motif previously established [7,9,1012]. Note Cys-59 is next to Asp-60. Right: An AlphaFold model of the *Sc*Dph1•Dph2 heterodimer (forest and limon green) confirming that cysteines in Dph1 (Cys-133; Cys-239; Cys-368) and Dph2 (Cys-C107; Cys-128; Cys-362) are proximal to respective Fe-S clusters. As part of TCMs, a fourth cysteine, Cys-134 next to Cys-133 in Dph1 and Cys-106 next to Cys-107 in Dph2, orients towards each Fe-S cluster. Fe-S motif close-ups are 66% transparent for emphasis on stick structures. Dph1•Dph2 was modelled and illustrated as previously described [10,21].

3.2. Diphthamide-Relevant Cooperation of Cys-106 & Cys-107 in the TCM of Dph2

Next, we examined the relevance, if any, of the TCMs (i.e., Dph1Cys-133 & Cys-134; Dph2Cys-106 & Cys-107) for diphthamide synthesis on eEF2 *in vivo*. We generated site-directed Cys-to-Ser substitution variants of Dph1•Dph2 containing individual and combined TCM replacements in subunits Dph1 (*C133S, C134S, C133,134S*) and Dph2 (*C106S, C107S, C106,107S*). For comparison, we included null-mutants (*dph1Δ*; *dph2Δ*) and Dph1•Dph2 variants (*dph1C239S*; *dph1C368S*; *dph2C362S*) with verified or suspected Fe-S ligand defects [9,10]. Next, diphthamide synthesis capacity was investigated *in vivo* with assays monitoring diphthamide-dependent cell growth inhibition by DT and sordarin (Figure 2A). The latter antifungal stalls ribosomes and blocks protein synthesis in a fashion unrelated to DT but also dependent on the diphthamide décor on eEF2 [38-40].
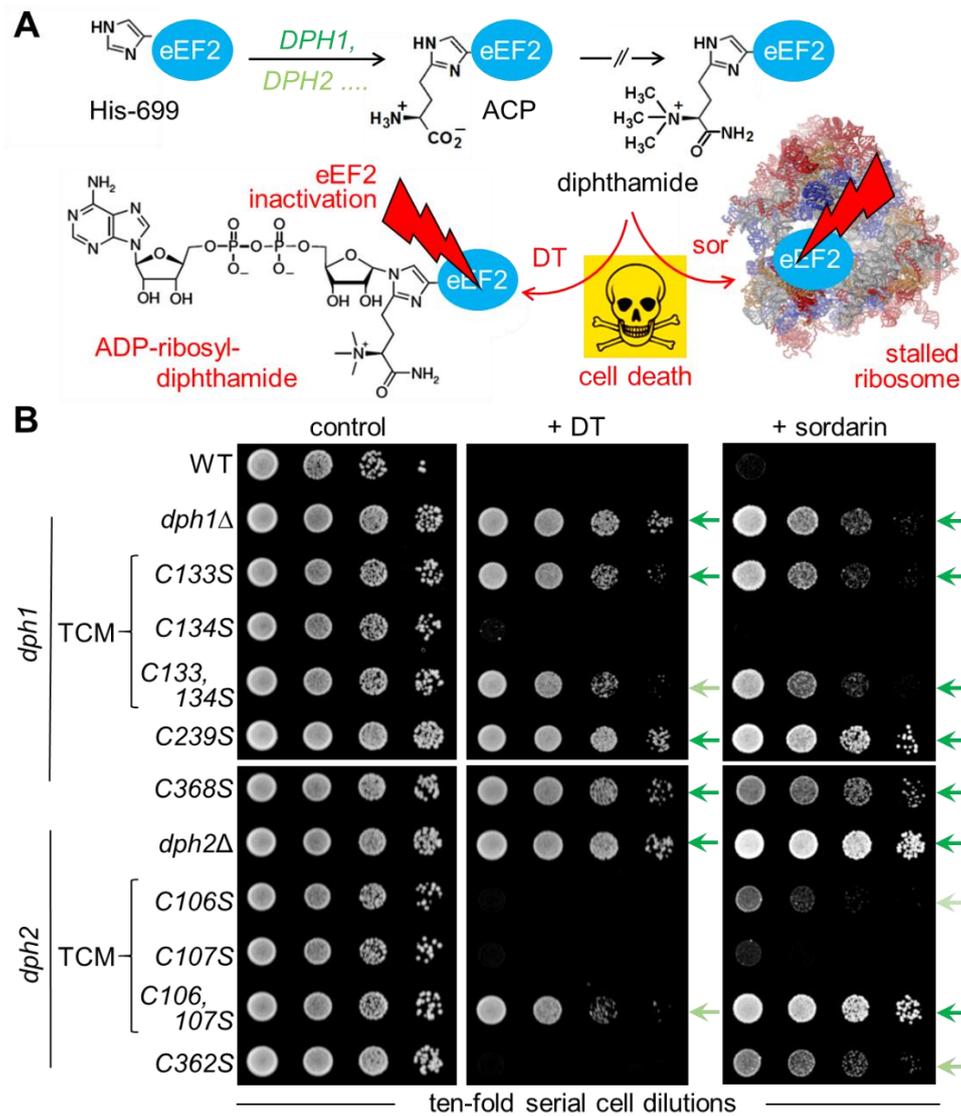
Figure 2. *DPH1* and *DPH2* mutagenesis to study TCM relevance for Dph1•Dph2 activity *in vivo*. (**A**) Simplified diphthamide pathway with *DPH1* and *DPH2* genes required to initiate ACP formation [21]; subsequent *DPH* products and steps for completion of diphthamide synthesis [14-17] are not detailed. Diphthamide can be hijacked to induce cell death (skull-crossbones) either by DT for lethal ADP-ribosylation of eEF2 or sordarin (sor), which in complex with the décor on eEF2 stalls ribosomes [40]. (**B**) Growth assays in response to DT and sordarin for diagnosis of diphthamide defects *in vivo*. Yeast tester strains comprised wild-type (WT: *DPH1 DPH2*) and null-mutants (*dph1Δ*; *dph2Δ*) together with single/double *DPH1* or *DPH2* gene substitutions as indicated. Cells were cultivated w/o DT and sordarin (control: left panel), under DT inducing conditions (+ DT: middle panel) [24] or with sordarin (+ sordarin: right panel) doses sufficient to inhibit WT cells. Arrows shaded in green denote various degrees of DT and sordarin resistance.

First, tester strains were transformed with pSU9, a plasmid allowing for expression of the catalytic DT subunit under *GAL1* promoter control [24]. Under inducing conditions, i.e., with galactose added to the growth medium as sole carbon source (Figure 2B), a sensitive DT phenotype leading to cell death was seen with diphthamide-proficient wild-type (WT) cells (Figure 2B). In contrast, DT resistance traits comparable to diphthamide-deficient *dph1Δ* and *dph2Δ* null-controls were found to be triggered by Cys-to-Ser substitution in the *DPH1* (*C133S*, *C133,134S*, *C239S*, *C386S*) and *DPH2* (*C106,107S*) genes (Figure 2B). Intriguingly, compared to the latter double mutant, which has both cysteines in the TCM of Dph2 replaced by serines (*C106,107S*), substitution of each cysteine

alone (*C106S* or *C107S*) did not protect either single mutant against DT (Figure 2B). This is a phenotypic read-out indicative for functional overlap between Cys-106 & Cys-107 in the TCM of Dph2. Consistently, functional cooperation among the two cysteines can also be deduced from (DT independent) assays that monitor resistance towards the diphthamide indicator antifungal sordarin [38-40]. Here, phenotypic additivity between Cys-106 & Cys-107 is even more pronouced (compared to the DT assay), and the double substitution mutant (*C106,107S*) conferred sordarin resistance as robust as the *dph2Δ* null-control lacking Dph1•Dph2 activity altogether (Figure 2B). This out-come significantly differs from the phenotypes triggered by the respective TCM substitutions in Dph1 (Figure 2B). While one of the single mutants (*C133S*) copies DT and sordarin resistance traits of the double mutant (*C133,134S*), the other single mutant (*C134S*) displayed WT-like sensitivities to either of the diphthamide indicator agents (Figure 2B). Thus, in the TCM of Dph1, Cys-133 apparently is the major catalytic driver, and Cys-134 plays no such role for diphthamide synthesis by the RS enzyme.

As with previously reported assays [10,24,32,39,41], we noticed that both DT and sordarin triggered phenocopies in most of our genetic backgrounds (Figure 2B), which is in further support of their use as *bona fide* diphthamide indicators. However, in case of the *DPH2* substitution (*C362S*), which when mutated together with Cys-106 (*C106,362A*) was reported to have a Fe-S cluster defect *in vitro* [9], we observed an exception from this principle, i.e., separation of DT sensitivity from sordarin resistance (Figure 2B). Whether such phenotypic heterogeneity is unique to the mutant (*C362S*) and reflects a specific difference in response to both cytotoxic agents, which in spite of sharing the requirement for diphthamide, have distinct *modi operandi* [23,40] is not known to the best of our knowledge. Nonetheless, it is feasible to this end that eEF2 diphthamide modification states sufficient to undergo lethal ADPR by DT (i.e., sensitivity phenotype) may not be enough to be targetable by sordarin and freeze eEF2 on the ribosome to kill yeast cells (i.e., resistance trait phenotype) [23,40].

3.3. Cys Substitutions in the SAM & Fe-S Motifs Trigger Unmodified eEF2 Pools

Next we analyzed the Cys-to-Ser variants using Western blots with anti-eEF2(no diphthamide) antibodies that specifically recognize unmodified eEF2 [31-33] (Figure 3A). Thus, in support of our phenotypic assays above (Figure 2B) such immune blots can provide further insights into the relevance of each cysteine replaced in our Dph1 or Dph2 substitution variants and confirm that modified eEF2 samples from WT cells with active Dph1•Dph2 enzyme will not respond towards this diagnostic antibody [31-33]. While our WT control contained next to no unmodified eEF2, the *dph1Δ* and *dph2Δ* deletion strains accumulated substantial pools of eEF2 not modified by diphthamide (Figure 3A). Based on this rationale, we detected pools of unmodified eEF2 in *DPH1* single *C133S*, *C239S* and *C368S* as well as double *C133,134S* mutants that compared to *dph1Δ* signals (Figure 3A, left panel). In contrast, eEF2 diphthamide modification states in the *DPH1* single substitution mutant *C134S* resembled WT pools bare of any unmodified eEF2 (Figure 3A, left panel). We conclude that in contrast to the robust defect seen with the *dph1C133S* mutant, the *C134S* substitution is fully proficient in diphthamide synthesis. This read-out, which complements our data from the DT and sordarin assays above (Figure 2B), reconfirms that within the TCM of Dph1, Cys-133 (not Cys-134) is the major diphthamide driver.

In relation to *DPH1*, the set of cysteine mutations in the *DPH2* gene uncovered a more complex functional profile (Figure 3A, right panel) that goes hand-in-hand with the *in vivo* phenotypes above (Figure 2B). Again, individual replacements of Cys-106 (*C106S*) and Cys-107 (*C107S*) within the TCM of Dph2 produced small pools of unmodified eEF2, yet to a significantly lesser degree than the *dph2Δ* null-control (Figure 3A right panel). In contrast, the double mutant (*C106,107S*) lacking the TCM in Dph2 altogether, triggered substantial amounts of unmodified eEF2 (Figure 3A right panel). In fact, the diphthamide defect seen for double mutant (*C106,107S*) cells compares to unmodified eEF2 pools from *dph2Δ* nulls and Fe-S ligand mutant (*C362S*) [9] (Figure 3A, right panel), which we showed above displays phenotypic heterogeneity (Figure 2B).
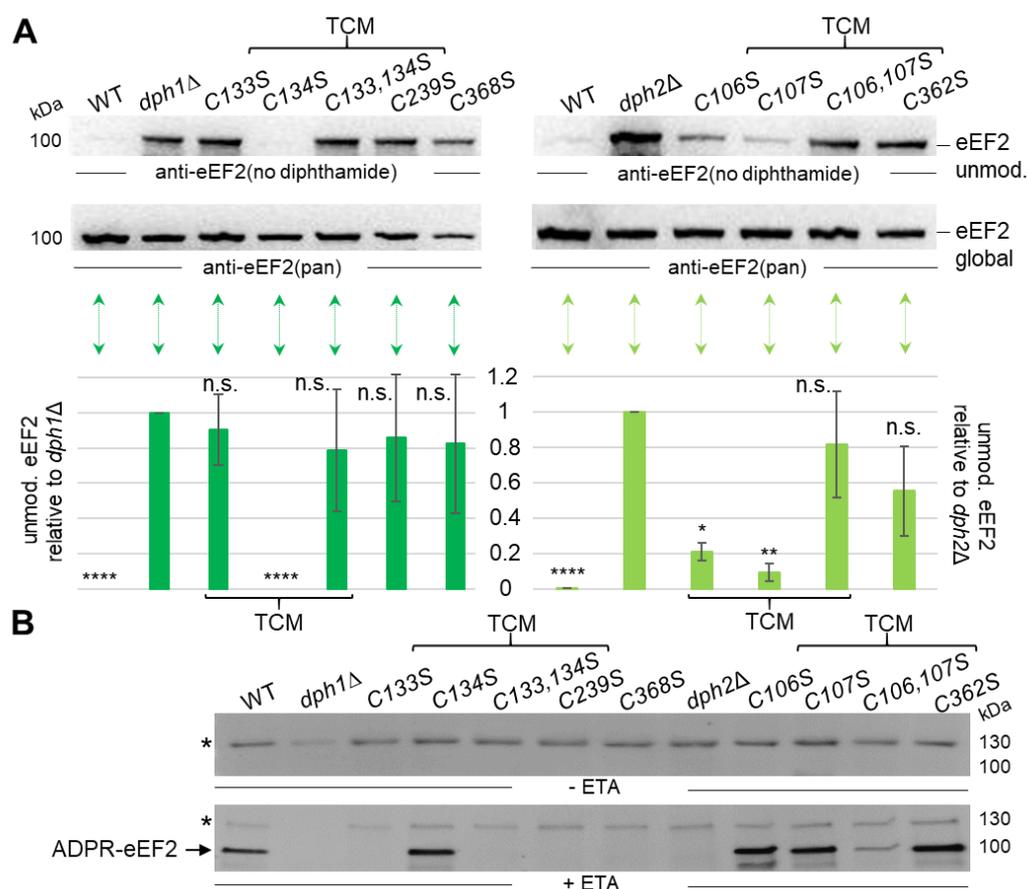
Figure 3. Accumulation of unmodified eEF2 in Cys-to-Ser Dph1•Dph2 mutants reveals functional roles of TCMs in diphthamide synthesis. (**A**) Western blots diagnostic for diphthamide synthesis on eEF2 from cell extracts of indicated yeast strains;anti-eEF2(no diphthamide) antibodies specific for unmodified eEF2 (upper panels), produce immune signals that associate with dysfunctional Dph1•Dph2 rather than WT enzyme, and anti-eEF2(pan) antibodies (middle panels) recognize eEF2 irrespective of modification state [31-33]. Technical repetitions (n=3) were quantified (lower panels) using t-test statistics (* = p<0.05; ** = p<0.01; **** = p<0.0001; n.s. = not significant). (**B**) ADP-ribosylation (ADPR) assay. Cell extracts incubated w/o (upper panel) or with exotoxin A (ETA) (500 ng, lower panel) with biotin-NAD+ allowed diphthamide-dependent biotin-ADP-ribose transfer (ADPR-eEF2). Detectionwas by Western blot using a streptavidin-HPR-conjugate. Asterisks mark an unspecific ADPR band previously described [24]. Original images can be found in Supplementary Materials (Figure S2, S3 and S4).

We next aimed to verify the Western blot data above using an independent assay *in vitro* [37] (Figure 3B). It is based on ETA, which similar to DT, requires the diphthamide décor to attack eEF2 by ADP-ribosylation in a reaction involving NAD+ as ADP-ribose donor (Figure 3B). In the assay, use of biotinylated NAD+ enables to monitor the ADPR modification on eEF2 through streptavidin-based Western blots [37]. Functionally compromised or inactive Dph1•Dph2 renders eEF2 unmodified and hence less sensitive or resistant to the ADPR attack by ETA, resulting in reduced or lack of Western signals in relation to WT cells with active Dph1•Dph2 enzyme (Figure 3A). While diphthamide-deficient *DPH1* mutants *C133S*, *C239S* and *C368S* displayed no ADPR acceptor band for eEF2, the *C134S* mutant showed WT-like ADPR patterns (Figure 3B). This finding, which is in line with the WT-like read-outs from the other assays above (Figure 2B and 3A), supports the view that Cys-134 is functionally dispensable from the TCM in Dph1. Markedly, ADPR signals on eEF2 observed in particular from *DPH2* mutants (*C106, 107S* and *C362S*) point towards detectable diphthamide levels (Figure 3B) even though *in vivo* phenotypes (Figure 2B) and anti-eEF2 Western blots implied diphthamide defects (Figure 3A). In spite of Cys-106 and Cys-362 being verified as Fe-S cluster

ligands in Dph2 that lose cooperativity when mutated in tandem (*C106,362A*) [9], we can thus conclude that Dph1•Dph2 activities in each of our single mutants (*C107S* or *C362S*) are decreased, not abolished. Thus, residual diphthamide levels produced from each mutant background may be sufficient enough to generate the observed pools of ADPR-eEF2. Such scenario is not unheard of and was reported before with regards to a subset of pathogenic and clinically important variants of DPH1•DPH2 from human DDS patients [10,19-21].

Strikingly, in relation to each single mutant (*C106S* or *C107S*) alone, eEF2 from the *DPH2* double substitution (*C106,107S*) variant displayed a drastic decrease in ADPR acceptor activity (Figure 3B). Again, this finding indicates a robust reduction in RS enzyme activity when both Cys residues of the TCM in Dph2 have been replaced by Ser residues (Figure 3B) and goes hand-in-hand with our data from the Western blots above, which demonstrate that Cys-106 and Cys-107 cooperate with one another and confer full functionality to the Dph1•Dph2 heterodimer. In sum, our TCM analysis in Dph1 demonstrates that while Cys-134 clearly is dispensable, Cys-133 is essential for Dph1•Dph2 enzyme activity and diphthamide synthesis on eEF2. Thus, together with previous studies on the atypical radical SAM domain in Dph1 [9,10], Cys-133 appears critical for Fe-S cluster coordination. As for Dph2, our TCM analysis and diphthamide profiles uncover that replacement of Cys-106 or Cys-107 alone results in partial loss of enzyme activity, while lack of both dramatically compromise Dph1•Dph2 function. Therefore, we propose a cooperative role between Cys-106 and Cys-107 in the TCM of Dph2 that likely supports Fe-S cluster binding and Dph1•Dph2 enzyme function.

3.4. Mutations in the SAM & Fe-S Motifs Drastically Decrease Dph1•Dph2 Amounts

Previously, yeast Dph1•Dph2 variants with Cys-to-Ala substitutions were reported with low protein yields when produced from recombinant bacteria [9]. In line with this, we reported that *DPH1* substitution mutant (*C368S*) produced significantly lower Dph1 amounts than WT cells [10]. Hence, we studied Dph1•Dph2 levels in our collection of mutants with HA and c-Myc epitope-tagged versions of the Cys-to-Ser variants generated by PCR-mediated protocols *in vivo* . Yeast strains co-expressing Dph1-HA variants with Dph2-c-Myc (Figure 4A and Figure S5) or Dph2-c-Myc variants with Dph1-HA (Figure S6 and S7) were analysed by Western blots using anti-HA and anti-c-Myc antibodies to detect each subunit in the Dph1•Dph2 populations. As for the *DPH1* set of mutations, cellular amounts of all HA-tagged Cys-to-Ser variants (*C133S*; *C133,134S*; *C239S*; *C368S*) – except for the one (*C134S*) with WT-like properties based on the assays above (Figure 2 and 3) – were significantly decreased (Figure 4A, left panel). In fact, Dph1-HA levels in all these mutants (*C133S*; *C133,134S*; *C239S*; *C368S*) had dropped to 25-38% (Figure 4A, right panel) of the WT control (*DPH1-HA DPH2-c-Myc*). Strikingly, we also observed a drastic decrease in their amounts of Dph2-c-Myc (Figure 4A, left panel). Thus, albeit encoded from otherwise native genomic *DPH2* loci, the Dph2-c-Myc levels had dropped to 13-27% of WT-levels (Figure 4A, right panel) in all *dph1* mutants (*C133S*; *C133,134S*; *C239S*; *C368S*). Again, the active (*C134S*) mutant deviated from this pattern producing proper or even higher than WT-pools of the epitope-tagged Dph1•Dph2 dimer (Figure 4A). Thus, dramatically reduced Dph1 and Dph2 protein levels occur in the very Cys-Ser substitutions of the *DPH1* gene product that interfere with the radical SAM motif in Dph1 and compromise diphthamide synthesis [9,10,42].

Similarly, we observed reduction of Dph1•Dph2 enzyme and subunit levels with the *DPH2* set of mutations (Figure S6 and S7), albeit not as severe as with the *dph1* mutant collection above (Figure 4A). Among *dph2* mutants tested (*C106S*; *C107S*; *C106,107S*; *C362S*), the levels of Dph2-c-Myc and Dph1-HA dropped to respectively 40-71% and 30-56% relative to WT (Figure S6 and S7). *dph2* mutants found to be severely compromised (*C106,107S*; *C362S*) in Dph1•Dph2 activity on the basis of phenotypic (Figure 2B), anti-eEF2 (Figure 3A), and ADPR (Figure 3B) assays, maintained Dph2-c-Myc or Dph1-HA at reduced but significant higher levels compared to the most affected *dph1* counterparts (*C133S*; *C133,134S*; *C239S*; *C368S*) (Figure 4A). This suggests that loss of the capacity to synthesize diphthamide in each of the mutant Dph1•Dph2 populations may not be solely ascribed to changed levels in Dph1 and/or Dph2 subunits. In support, we observe significantly lesser Dph1•Dph2 instability in the inactive *dph2C362S-c-Myc DPH1-HA* mutant (Figure S6 and S7), which

according to Dong *et al*. (2019) is malfunctional due to a binding defect of a regulatory rather than catalytic Fe-S cluster Dph2 [9].
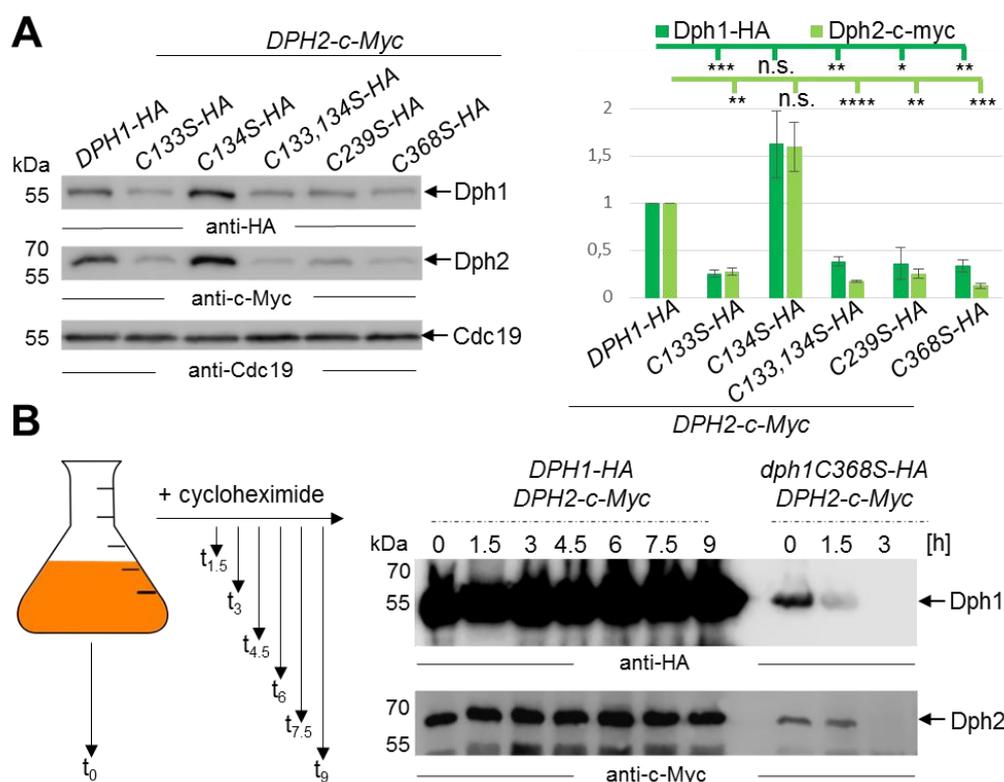

Figure 4. Malfunctional Cys-to-Ser variants of the Dph1•Dph2 dimer have significantly decreased amounts of Dph1 and Dph2 subunits. (**A**) Western blot detection of Dph1-HA (anti-HA) and Dph2-c-Myc (anti-c-Myc) from total extracts of indicated *DPH1-HA* substitution mutants co-expressing *DPH2-c-Myc* (left panel). Detection of Cdc19 (anti-Cdc19) served as internal control. Technical repetitions (n=3) were followed by densitometric quantification of signal intensities (right panel) and t-test statistics (* = p<0.05; ** = p<0.01; *** = p<0.001; **** = p<0.0001; n.s. = not significant). (**B**) Cycloheximide chase of *dph1C368S* reveals accelerated decay of Dph1•Dph2. Schematic workflow of the cycloheximide chase (left panel). Yeast cells coding for HA and c-Myc tagged Dph1 and Dph2 were grown to exponential phase (t_0) before addition of cycloheximide. Samples were taken at indicated time points before (t0) and after cycloheximide addition for protein extraction and Western blot analysis (right panel). Original images can be found in Supplementary Materials (Figure S5 and S8).

3.5. Non-Canocical SAM Motifs Ensure Dph1•Dph2 Stability in Yeast Cells over Time

To further address Dph1•Dph2 instability as a direct or indirect result from Cys-to-Ser substitutions in the *DPH1* or *DPH2* gene products (Figure 4A), we chose a cycloheximide chase experiment [36] followed by Western blots (Figure 4B). Cycloheximide inhibits translation in eukaryotes in a fashion involving competition with the acceptor end of deacetylated tRNA in the ribosome [43,44]. Eventually, translation becomes stalled as uncharged tRNAs remain stuck and block *de novo* protein synthesis. As proteins including Dph1 and Dph2 lack replenishment after cycloheximide treatment, their stability *versus* degradation can be readily traced over time in Western blots (Figure 4B). We grew WT (*DPH1-HA DPH2-c-Myc*) and mutant (*dph1C368-HA DPH2-c-Myc*) yeast strains to exponential phase before applying cycloheximide (100 µg/ml) for up to nine hours (Figure 4B and Figure S8). Total extracts from the resulting fractions were subjected to Western blots using anti-HA and anti-c-Myc antibodies to detect either subunit of Dph1•Dph2 (Figure 4B). While we observed no change in Dph1-HA (anti-HA) or Dph2-c-Myc (anti-c-Myc) over nine hours from WT cells, both subunits of the heterodimer from diphthamide mutant *dph1C368S* vanished unanimously

after three hours into the cycloheximide chase (Figure 4B). Similarly, we examined Dph1•Dph2 instability upon chasing the *dph2* double Cys-to-Ser variant (*C106,107S-c-Myc DPH1-HA*) by cycloheximide. Although Dph1•Dph2 levels decreased over time as a result of the combined (*C106,107S*) substitutions in the TCM of Dph2 (Figure S9 and S10), Dph1-HA and Dph2-c-Myc protein instability appeared significantly less prominent compared to the critical *dph1* mutant above (Figure 4B). Thus, after three hours into the cycloheximide chase, relative stable subunit pools amounted to 69% (Dph1-HA) and 55% (Dph2-c-Myc) (Figure S9 and S10). In sum, Dph1•Dph2 instability is enhanced in either background, and subunit degradation that associates with Cys-to-Ser substitutions, is predominantly seen and prone to alterations in the Fe-S cluster motif from Dph1, which likely is site-differentiated for SAM binding and cleavage by the Dph1•Dph2 enzyme [9,10,21,42].

4. Conclusion and Perspectives

In this study, we further analysed atypical radical SAM and Fe-S motifs of Dph1•Dph2, a non-canonical RS enzyme from yeast. We focused primarily on hitherto ill-defined cysteines in Dph1 (Cys-134) and Dph2 (Cys-106) that form TCMs conserved in eukaryotic members of the Dph1•Dph2 heterodimer (Figure 1). We were able to rule out functional relevance for Dph1Cys-134 in the diphthamide modification pathway. However, we found that loss of Dph2Cys-107 (mild enzyme defect when substituted alone for Ser) together with Dph2Cys-106 (also weak diphthamide defect on its own) renders yeast cells almost unable to synthesize diphthamide on eEF2. Congruently, eEF2 from the double mutant (*C106,107S*) accumulates unmodified eEF2 (Figure 2) that hardly has acceptor activity for ADP-ribosylation, a diphthamide-dependent modification reaction (Figure 3). Previously, Dong et al. (2019) identified Fe-S cluster binding roles for Cys-107, Cys-128 and Cys-362 in the Dph2 subunit and suggested for Cys-106 a potential fourth ligand role [9]. Our data presented in-here are in strong support of this option, and we show that Cys-106 & Cys-107 indeed functionally overlap in the TCM of Dph2 and contribute to full Dph1•Dph2 enzyme activity. In line with cooperativity, the double mutant (*C106,107S*) triggers phenotypes and properties that add-up in relation to each single mutant (*C106S* or *C107S*) indicating a *bone fide* diphthamide defect *in vivo* (Figure 2 and 3).

To further put our data into perspective, we revisited structural models of the cofactor binding motifs in the Dph1•Dph2 heterodimer (Figure 1). We compared the distance between iron ions and proximal cysteines in the TCMs of Dph1 (Cys-133: 1.5 Å, essential residue; Cys-134: 3.9 Å, non-essential residue) (Figure S11) in comparison to the TCM in Dph2, (cooperating residues Cys-106: 2.0 Å and Cys-107: 3.0 Å). Obviously, the latter two share closer distances towards the nearest iron ion in the Fe-S cluster model, which supports our data reinforcing a functional overlap between Cys-106 & Cys-107 in Dph2 (but not Cys-133 & Cys-134 in Dph1) (Figure S11). Other microbial Fe-S cluster containing proteins like NuoB ligate two irons with two tandem cysteines [45,46]. In case of Dph2, such a modified stoichiometry ($CCX_{21}CX_{234}C$) may update and expand the Fe-S cluster ligands to Cys-106, Cys-107, Cys128 & Cys-362 (Figure 1B). If this is the case, the cofactor not necessarily exposes a unique, Cys-free iron typical of site-differentiated radical SAM motifs required for binding and cleavage of the cosubstrate SAM [1-4]. This notion is in line with recent genetic and biochemical evidence [9,10,42] showing that subunit Dph1 (not Dph2) contains a functional SAM pocket in the Dph1•Dph2 dimer. Irrespective of these novel insights, further studies will be required to elucidate Fe-S cluster function in the Dph2 subunit of the asymmetric RS enzyme. Previous evidence suggested it is necessary for Dph1•Dph2 activation by the iron-binding and electron carrier protein Dph3 (aka Kti11) [47-50], which in complex with Dph8 (aka Kti13) also acts on Elongator, another translation-relevant RS enzyme complex that modifies tRNA anticodons [51-53]. However, activation details remain unclear to this end.

Nonetheless, our data identify cysteines in the TCM of Dph2 (Cys-106 & Cys-107) that cooperate in Dph1•Dph2 functionality and found Cys-133 in the TCM of Dph1 is particular critical for the structural integrity of the dimeric RS enzyme. Likewise, other Cys residues in the non-canonical radical SAM motif of Dph1 (Cys-239; Cys-368) ensure Dph1•Dph2 stability, suggesting both

cofactor/cluster motifs in the Dph1 and Dph2 subunits communicate on the level of enzyme integrity and stability. Thus, as with viperin, and other medically relevant classical RS enzyme, structural integrity of the non-canonical RS enzyme Dph1•Dph2 also relies on functional binding sites for SAM and Fe-S cofactors [4,6,54]. Intriguingly, clinically relevant human DPH1•DPH2 variants include a Tyr replacement in DPH2Cys-342, which in yeast corresponds to Dph2Cys-362 and was identified to be inactive upon Tyr substitution [21,22], likely through Fe-S cluster loss and enhanced protein instability. Thus, insights into the consequences of Cys-based cofactor motif substitutions as reported in-here can further address the critical roles diphthamide modification on eEF2 plays for accurate mRNA translation and protein synthesis in eukaryotes [55-58] and importantly, help understand molecular causes of pathogenic mutants for diagnosis of patients with DDS symptoms [18-22]. Last but not least, together with the recent discovery of another non-canonical RS enzyme that uses ACP rather than classical dAdo radicals for arsinothricin biosynthesis [59], our report reinforces both the diversity and emerging plasticity of radical SAM family members.

References

1. Frey, P.A.; Hegeman, A.D.; Ruzicka, F.J. The radical SAM superfamily. C_rit. Rev. Biochem. Mol. Biol._ **2008**, _43_, 63–88, doi: 10.1080/10409230701829169.
2. Hoffman, B.M.; Broderick, W.E.; Broderick, J.B. Mechanism of radical initiation in the radical SAM enzyme superfamily. _Annu. Rev. Biochem._ **2023**, _92_, 333–349, doi: 10.1146/annurev-biochem-052621-090638.
3. Yokoyama, K.; Lilla, E.A. C-C bond forming radical SAM enzymes involved in the construction of carbon skeletons of cofactors and natural products. _Nat. Prod. Rep._ **2018**, _35_, 660–694, doi: 10.1039/c8np00006a.
4. Nicolet, Y. Structure–function relationships of radical SAM enzymes. _Nat. Catal._ **2020**, _3_, 337–350, doi: 10.1038/s41929-020-0448-7.

5. Broderick, J.B.; Duffus, B.R.; Duschene, K.S.; Shepard, E.M. Radical S-adenosylmethionine enzymes. *Chem. Rev.* **2014**, *114*, 4229–4317, doi: 10.1021/cr4004709.

6. Haldar, S.; Paul, S.; Joshi, N.; Dasgupta, A.; Chattopadhyay, K. The presence of the iron-sulfur motif is important for the conformational stability of the antiviral protein, Viperin. *PLoS One* **2012**, *7*, e31797, doi: 10.1371/journal.pone.0031797.

7. Zhang, Y.; Zhu, X.; Torelli, A.T.; Lee, M.; Dzikovski, B.; Koralewski, R.M.; Wang, E.; Freed, J.; Krebs, C.; Ealick, S.E., Lin, H. Diphthamide biosynthesis requires an organic radical generated by an iron-sulphur enzyme. *Nature* **2010**, *465*, 891–896, doi: 10.1038/nature09138.

8. Broderick, J.B. Biochemistry: a radically different enzyme. *Nature* **2010**, *465*, 877–878, doi: 10.1038/465877a.

9. Dong, M.; Dando, E.E.; Kotliar, I.; Su, X.; Dzikovski, B.; Freed, J.H.; Lin, H. The asymmetric function of Dph1-Dph2 heterodimer in diphthamide biosynthesis. *J. Biol. Inorg. Chem.* **2019**, *24*, 777–782, doi: 10.1007/s00775-019-01702-0.

10. Ütkür, K.; Schmidt, S.; Mayer, K.; Klassen, R.; Brinkmann, U.; Schaffrath, R. *DPH1* Gene mutations identify a candidate SAM pocket in radical enzyme Dph1•Dph2 for diphthamide synthesis on EF2. *Biomolecules* **2023**, *13*, 1655, doi: 10.3390/biom13111655.

11. Lin, H. S-Adenosylmethionine-dependent alkylation reactions: when are radical reactions used? *Bioorg. Chem.* **2011**, *39*, 161–170, doi: 10.1016/j.bioorg.2011.06.001.

12. Zhu, X.; Dzikovski, B.; Su, X.; Torelli, A.T.; Zhang, Y.; Ealick, S.E.; Freed, J.H.; Lin, H. Mechanistic understanding of *Pyrococcus horikoshii* Dph2, a [4Fe-4S] enzyme required for diphthamide biosynthesis. *Mol. Biosyst.* **2011**, *7*, 74–81, doi: 10.1039/c0mb00076k.

13. Dong, M.; Kathiresan, V.; Fenwick, M.K.; Torelli, A.T.; Zhang, Y.; Caranto, J.D.; Dzikovski, B.; Sharma, A.; Lancaster, K.M.; Freed, J.H.; Ealick, S.E.; Hoffman, B.M.; Lin H. Organometallic and radical intermediates reveal mechanism of diphthamide biosynthesis. *Science* **2018**, *359*, 1247–1250, doi: 10.1126/science.aao6595.

14. Su, X.; Lin, Z.; Lin, H. The biosynthesis and biological function of diphthamide. *Crit. Rev. Biochem. Mol. Biol.* **2013**, *48*, 515–521, doi: 10.3109/10409238.2013.831023.

15. Liu, S.; Milne, G.T.; Kuremsky, J.G.; Fink, G.R.; Leppla, S.H. Identification of the proteins required for biosynthesis of diphthamide, the target of bacterial ADP-ribosylating toxins on translation elongation factor 2. *Mol. Cell. Biol.* **2004**, *24*, 9487–9497, doi: 10.1128/MCB.24.21.9487-9497.2004.

16. Tsuda-Sakurai, K; Miura, M. The hidden nature of protein translational control by diphthamide: the secrets under the leather. *J. Biochem.* **2019**, *165*, 1–8, doi: 10.1093/jb/mvy071.

17. Arend, M.; Ütkür, K.; Hawer, H.; Mayer, K.; Ranjan, N.; Adrian, L.; Brinkmann, U.; Schaffrath, R. Yeast gene *KTI13* (alias *DPH8*) operates in the initiation step of diphthamide synthesis on elongation factor 2. *Microb. Cell* **2023**, *10*, 195–203, doi: 10.15698/mic2023.09.804.

18. Urreizti, R.; Mayer, K.; Evrony, G.D.; Said, E.; Castilla-Vallmanya, L.; Cody, N.A.L.; Plasencia, G.; Gelb, B.D.; Grinberg, D.; Brinkmann, U.; et al. DPH1 syndrome: Two novel variants and structural and functional analyses of seven missense variants identified in syndromic patients. *Eur. J. Hum. Genet.* **2020**, *28*, 64–75, doi: 10.1038/s41431-019-0374-9.

19. Hawer, H.; Mendelsohn, B.A.; Mayer, K.; Kung, A.; Malhotra, A.; Tuupanen, S.; Schleit, J.; Brinkmann, U.; Schaffrath, R. Diphthamide-deficiency syndrome: A novel human developmental disorder and ribosomopathy. *Eur. J. Hum. Genet.* **2020**, *28*, 1497–1508, doi: 10.1038/s41431-020-0668-y.

20. Shankar, S.P.; Grimsrud, K.; Lanoue, L.; Egense, A.; Willis, B.; Hörberg, J.; AlAbdi, L.; Mayer, K.; Ütkür, K.; Monaghan, K.G.; et al. A novel DPH5-related diphthamide-deficiency syndrome causing embryonic lethality or profound neurodevelopmental disorder. *Genet. Med.* **2022**, *24*, 1567–1582, doi: 10.1016/j.gim.2022.03.014

21. Ütkür, K.; Mayer, K.; Khan, M.; Manivannan, T.; Schaffrath, R.; Brinkmann, U. DPH1 and DPH2 variants that confer susceptibility to diphthamide deficiency syndrome in human cells and yeast models. *Dis. Model. Mech.* **2023**, *16*, dmmm050207, doi: 10.1242/dmm.050207.

22. Schaffrath, R.; Brinkmann, U. Diphthamide - a conserved modification of eEF2 with clinical relevance. *Trends Mol. Med.* **2024**, *30*, 164–177, doi: 10.1016/j.molmed.2023.11.008.

23. Jørgensen, R.; Merrill, A.R.; Andersen, G.R. The life and death of translation elongation factor 2. *Biochem. Soc. Trans.* **2006**, *34*, 1–6. doi: 10.1042/BST20060001.

24. Uthman, S.; Bär, C.; Scheidt, V.; Liu, S.; ten Have, S.; Giorgini, F.; Stark, M.J.R.; Schaffrath, R. The amidation step of diphthamide biosynthesis in yeast requires *DPH6*, a gene identified through mining the *DPH1-DPH5* interaction network. *PLoS Genet.* **2013**, *9*, e1003334, doi: 10.1371/journal.pgen.1003334.

25. Toulmay, A.; Schneiter, R. A Two-step method for the introduction of single or multiple defined point mutations into the genome of *Saccharomyces cerevisiae*. *Yeast* **2006**, *23*, 825–831, doi: 10.1002/yea.1397.

26. Janke, C.; Magiera, M.M.; Rathfelder, N.; Taxis, C.; Reber, S.; Maekawa, H.; Moreno-Borchart, A.; Doenges, G.; Schwob, E.; Schiebel, E.; et al. A versatile toolbox for PCR-based tagging of yeast genes: New fluorescent proteins, more markers and promoter substitution cassettes. *Yeast* **2004**, *21*, 947–962, doi:10.1002/yea.1142.

27. Daniel Gietz, R.; Woods, R.A.; Gietz, R.D.; Woods, R.A. Transformation of yeast by lithium acetate/single-stranded carrier DNA/polyethylene glycol method. *Methods Enzymol* **2002**, *350*, 87–96, doi:10.1016/S0076-6879(02)50957-5.

28. Sherman, F. Getting started with yeast. Methods Enzymol. **2002**, 350, 3–41, doi: 10.1016/s0076-6879(02)50954-x.

29. Jumper, J.; Evans, R.; Pritzel, A.; Green, T.; Figurnov, M.; Ronneberger, O.; Tunyasuvunakool, K.; Bates, R.; Žídek, A.; Potapenko, A.; et al. Highly accurate protein structure prediction with AlphaFold. *Nature* **2021**, *596*, 583–589, doi: 10.1038/s41586-021-03819-2.

30. Mirdita, M.; Schütze, K.; Moriwaki, Y.; Heo, L.; Ovchinnikov, S.; Steinegger, M. ColabFold: Making protein folding accessible to all. *Nat. Methods* **2022**, *19*, 679–682, doi: 10.1038/s41592-022-01488-1.

31. Stahl, S.; Da Silva Mateus Seidl, A.R.; Ducret, A.; Kux van Geijtenbeek, S.; Michel, S.; Racek, T.; Birzele, F.; Haas, A.K.; Rueger, R.; Gerg, M.; et al. Loss of diphthamide pre-activates NF-KB and death receptor pathways and renders MCF7 cells hypersensitive to tumor necrosis factor. *Proc. Natl. Acad. Sci. USA* **2015**, *112*, 10732–10737, doi: 10.1073/pnas.1512863112.

32. Hawer, H.; Ütkür, K.; Arend, M.; Mayer, K.; Adrian, L.; Brinkmann, U.; Schaffrath, R. Importance of diphthamide modified EF2 for translational accuracy and competitive cell growth in yeast. *PLoS One* **2018**, *13*, e0205870, doi:10.1371/journal.pone.0205870.

33. Zhang H, Quintana J, Ütkür K, Adrian L, Hawer H, Mayer K, Gong X, Castanedo L, Schulten A, Janina N, Peters M, Wirtz M, Brinkmann U, Schaffrath R, and Krämer U. Translational fidelity and growth of *Arabidopsis* require stress-sensitive diphthamide biosynthesis. *Nat. Comm.* **2022**, *13*, 4009, doi: 10.1038/s41467-022-31712-7.

34. Zachariae, W.; Shin, T.H.; Galova, M.; Obermaier, B.; Nasmyth, K. Identification of subunits of the anaphase-promoting complex of *Saccharomyces cerevisiae*. *Science* **1996,** *274*, 201–1204, doi: 10.1126/science.274.5290.1201.

35. Bradford, M.M. A rapid and sensitive method for the quantitation of microgram quantities of protein utilizing the principle of protein-dye binding. *Anal. Chem.* **1976**, *72*, 248–254. doi: 10.1006/abio.1976.9999.

36. Buchanan, B.W.; Lloyd, M.E.; Engle, S.M.; Rubenstein, E.M. Cycloheximide chase analysis of protein degradation in *Saccharomyces cerevisiae*. *J. Vis. Exp.* **2016**, *110*, 53957, doi: 10.3791/53975

37. Mayer, K.; Schröder, A.; Schnitger, J.; Stahl, S.; Brinkmann, U. Influence of DPH1 and DPH5 protein variants on the synthesis of diphthamide, the target of ADP-ribosylating toxins. *Toxins* **2017**, *9*, 78, doi: 10.3390/toxins9030078.

38. Botet, J.; Rodriguez-Mateos, M.; Ballesta, J.P.; Revuelta, J.L.; Remacha, M. A chemical genomic screen in *Saccharomyces cerevisiae* reveals a role for diphthamidation of translation elongation factor 2 in inhibition of protein synthesis by sordarin. *Antimicrob. Agents Chemother.* **2008**, *52*, 1623–1629. doi: 10.1128/AAC.01603-07.

39. Bär, C.; Zabel, R.; Liu, S.; Stark, M.J.; Schaffrath, R. A versatile partner of eukaryotic protein complexes that is involved in multiple biological processes: Kti11/Dph3. *Mol. Microbiol.* **2008**, *69*, 1221–1233, doi: 10.1111/j.1365-2958.2008.06350.x.

40. Shao, Y.; Molestak, E.; Su, W.; Stankevič, M.; Tchórzewski, M. Sordarin – an anti-fungal antibiotic with a unique modus operandi. *Br. J. Pharmacol.* **2022,** *179*, 1125–1145, doi: 10.1111/bph.15724.

41. Abdel-Fattah, W.; Scheidt, V.; Uthman, S.; Stark, M.J.R.; Schaffrath, R. Insights into diphthamide, key diphtheria toxin effector. *Toxins* **2013**, *5*, 958–968, doi: 10.3390/toxins5050958.

42. Fenwick, M.K.; Dong, M.; Lin, H.; Ealick, S.E. The crystal structure of Dph2 in complex with elongation factor 2 reveals the structural basis for the first step of diphthamide biosynthesis. *Biochemistry* **2019**, *58*, 4343–4351, doi: 10.1021/acs. biochem.9b00718.

43. Garreau De Loubresse, N.; Prokhorova, I.; Holtkamp, W.; Rodnina, M. V.; Yusupova, G.; Yusupov, M. Structural basis for the inhibition of the eukaryotic ribosome. *Nature* **2014**, *513*, 517–522, doi: 10.1038/nature13737.

44. Susorov, D.; Zakharov, N.; Shuvalova, E.; Ivanov, A.; Egorova, T.; Shuvalov, A.; Shatsky, I.N.; Alkalaeva, E. Eukaryotic translation elongation factor 2 (eEF2) catalyzes reverse translocation of the eukaryotic ribosome. *J. Biol. Chem.* **2018**, *293*, 5220–5229, doi: 10.1074/jbc.RA117.000761.

45. Schimpf, J.; Oppermann, S.; Gerasimova, T.; Santos Seica, A.F.; Hellwig, P.; Grishkovskaya, I.; Wohlwend, D.; Haselbach, D.; Friedrich, T. Structure of the peripheral arm of a minimalistic respiratory complex I. *Structure* **2022**, *30*, 80–94. e4, doi: 10.1016/j.str.2021.09.005.

46. Duarte, M.; Pópulo, H.; Videira, A.; Friedrich, T.; Schulte, U. Disruption of iron-sulphur cluster N2 from NADH: ubiquinone oxidoreductase by site-directed mutagenesis. *Biochem. J.* **2002**, *364*, 833–839, doi:10.1042/BJ20011750.

47. Sun, J.; Zhang, J.; Wu, F.; Xu, C.; Li, S.; Zhao, W.; Wu, Z.; Wu, J.; Zhou, C.Z.; Shi, Y. Solution structure of Kti11p from *Saccharomyces cerevisiae* reveals a novel zinc-binding module. *Biochemistry* **2005,** *44*, 8801–8809, doi: 10.1021/bi0504714.

48. Proudfoot, M.; Sanders, S.A.; Singer, A.; Zhang, R.; Brown, G.; Binkowski, A.; Xu, L.; Lukin, J.A.; Murzin, A.G.; Joachimiak, A.; Arrowsmith, C.H.; Edwards, A.M.; Savchenko, A.V.; Yakunin, A.F. Biochemical and structural characterization of a novel family of cystathionine beta-synthase domain proteins fused to a Zn ribbon-like domain. *J. Mol. Biol.* **2008**, *375*, 301–315, doi: 10.1016/j.jmb.2007.10.060.

49. Dong, M.; Su, X.; Dzikovski, B.; Dando, E.E.; Zhu, X.; Du, J.; Freed, J.H.; Lin, H. Dph3 is an electron donor for Dph1-Dph2 in the first step of eukaryotic diphthamide biosynthesis. *J. Am. Chem. Soc.* **2014**, *136*, 1754–1757, doi: 10.1021/ja4118957.

50. Zhang, Y.; Su, D.; Dzikovski, B.; Majer, S.H.; Coleman, R.; Chandrasekaran, S.; Fenwick, M.K.; Crane, B.R.; Lancaster, K.M.; Freed, J.H.; Lin, H. Dph3 enables aerobic diphthamide biosynthesis by donating one iron atom to transform a [3Fe-4S] to a [4Fe-4S] cluster in Dph1-Dph2. *J. Am. Chem. Soc*. **2021**, *143*, 9314–9319, doi: 10.1021/jacs.1c03956.

51. Lin, Z.; Dong, M.; Zhang, Y.; Lee, E.A.; Lin, H. Cbr1 is a Dph3 reductase required for the tRNA wobble uridine modification. *Nat. Chem. Biol*. **2016**, *12*, 995–997, doi: 10.1038/

52. Glatt, S.; Zabel, R.; Vonkova, I.; Kumar, A.; Netz, D.J.; Pierik, A.J.; Rybin, V.; Lill, R.; Gavin, A.C.; Balbach, J.; Breuing, K.D.; Müller C.W. Structure of the Kti11/Kti13 heterodimer and its double role in modification of tRNA and eukaryotic elongation factor 2. *Structure* **2015**, *23*, 149–160, doi: 10.1016/j.str.2014.11.008.

53. Kolaj-Robin, O.; McEwen, A.G.; Cavarelli, J.; Séraphin, B. Structure of the Elongator cofactor complex Kti11/Kti13 provides insight into the role of Kti13 in Elongator-dependent tRNA modification. *FEBS J.* **2015**, *282*, 819–833, doi: 10.1111/febs.13199.

54. Landgraf, B.J.; McCarthy, E.L.; Booker, S.J. Radical S-adenosylmethionine enzymes in human health and disease. *Annu. Rev. Biochem.* **2016**, *85*, 485–514, doi:10.1146/annurev-biochem-060713-035504.

55. Pellegrino, S.; Demeshkina, N.; Mancera-Martinez, E.; Melnikov, S.; Simonetti, A.; Myasnikov, A.; Yusupov, M.; Yusupova, G.; Hashem, Y. Structural insights into the role of diphthamide on elongation factor 2 in mRNA reading-frame maintenance. *J. Mol. Biol.* **2018**, *430*, 2677–2687, doi: 10.1016/j.jmb.2018.06.006.

56. Djumagulov, M.; Demeshkina, N.; Jenner, L.; Rozov, A.; Yusupov, M.; Yusupova, G. Accuracy mechanism of eukaryotic ribosome translocation. *Nature* **2021**, *600*, 543–546, doi: 10.1038/s41586-021-04131-9.

57. Milicevic, N.; Jenner, L.; Myasnikov, A.; Yusupov, M.; Yusupova, G. mRNA reading frame maintenance during eukaryotic ribosome translocation. *Nature* **2024**, *625*, 393–400, doi: 10.1038/s41586-023-06780-4.

58. Shin, B.-S.; Ivanov, I.P.; Kim, J.-R.; Cao, C.; Kinzy, T.G.; Dever, T.E. eEF2 diphthamide modification restrains spurious frameshifting to maintain translational fidelity. *Nucleic Acids Res.* **2023**, *51*, 6899–6913, doi: 10.1093/nar/gkad461.

59. Yao, Y.; He, J.; Dong, M. Arsinothricin biosynthesis involving a non-canonical radical SAM enzyme for C-As bond formation. *bioRxiv* **2024**, 2024.02.01.577332, doi: 10.1101/2024.02.01.577332.